Inclusive πd breakup reactions

Humberto Garcilazo*
Institut für Theoretische Physik, Universität Hannover, D-3000 Hannover 1, Federal Republic of Germany
(Received 7 August 1991; revised manuscript received 22 October 1992)

The inelastic reactions $^2H(\pi^+,\pi^+)X$, $^2H(\pi^-,\pi^0)X$, $^2H(\pi^+,p)X$, and $^2H(\pi^-,p)X$ are studied within a relativistic three-body model. Single and double differential cross sections are calculated and compared with available data and predictions are made where no data exist. Several approximate theoretical prescriptions are compared with the full calculation as well as the results from two different deuteron wave functions.

PACS number(s): 25.80.Gn, 13.75.Gx, 21.45.+v

I. INTRODUCTION

Pion-deuteron breakup processes have been studied extensively during the last ten years [1–12]. Kinematically complete experiments have been performed to measure the differential cross section [1,2,6,8,10–12] and the vector analyzing power [5,7,9] covering large regions of the available three-body phase space. In these kinds of experiments at least two particles must be detected; usually the proton and the pion in the case of the normal breakup [1–11] or the two protons in the case of the charge exchange reaction [12].

In contrast, the inclusive breakup processes require the detection of only one particle in the final state and are therefore much easier to study experimentally. It is thus somewhat a paradox that much less data exist on them: just a few differential cross sections [13–18] and no polarization data of any kind. In this paper we will describe a formalism to calculate the complete set of observables corresponding to an initially polarized deuteron. We will then apply this formalism to compare the predictions of our model with the existing differential cross section data as well as to present predictions where no data exist. We will explore the sensitivity of the inclusive πd breakup reactions to higher-order effects and to the use of different deuteron wave functions.

The inclusive πd breakup reactions are the link between the elastic πd process and the kinematically complete breakup reactions. Thus, they constitute an essential part of the πd system and must also be studied if one aims at a complete understanding of this system.

II. FORMALISM

A. Relativistic three-body model

If we call the pion particle 1 and the two nucleons particles 2 and 3, the relativistic Faddeev equations for πd elastic and inelastic scattering are written as

$$T_i=(1-\delta_{i1})t_i+\sum_{j\neq i} t_i G_k T_j \ , \tag{1}$$

where t_i is the off-shell scattering amplitude of particles j and k and G_k is the propagator of the exchanged particle k, that is, $i\neq k\neq j$. The integral equations (1) correspond to the spectator-on-mass-shell prescription in which all the spectator particles in the initial, final, and intermediate states are required to be on their mass shells [19,20]. Since the spectator-on-mass-shell condition eliminates the fourth component in the loop integrations of the intermediate states, Eqs. (1) are three-dimensional integral equations with the same degree of complexity as the usual nonrelativistic Faddeev equations. The operator describing πd breakup is

$$A=T_1+T_2+T_3 \ , \tag{2}$$

where the physical amplitude is obtained by taking the matrix elements of this operator between the initial state wave function consisting of a free pion times a np bound state and the final state wave function consisting of three free particles.

The impulse approximation corresponds to taking just the single scattering terms, that is,

$$A^{\mathrm{IA}}=t_2+t_3 \ , \tag{3}$$

since the Faddeev amplitude T_1 does not contribute in first order, that is,

$$T_1=t_1G_3T_2+t_1G_2T_3 \ . \tag{4}$$

If one uses in Eqs. (2) and (4) the single-scattering approximation for T_2 and T_3, Eq. (2) corresponds to the distorted-wave impulse approximation

$$A^{\mathrm{DWIA}}=(1+t_1G_3)t_2+(1+t_1G_2)t_3 \ , \tag{5}$$

since

$$\langle \mathbf{p}|(1+t_1G_k)\equiv\langle\chi^{(-)}_{\mathbf{p}}| \ , \tag{6}$$

is a nucleon-nucleon distorted wave of relative momentum $\mathbf{p}$.

We now introduce the quasiparticle or isobar approximation for the two-body amplitudes t_i as [19]

*Present address: Instituto de Estructura de la Materia, Consejo Superior de Investigaciones Científicas, Serrano 119, E-28006 Madrid, Spain.

$$t_i(s_i)=\sum_{m_i=-j_i}^{j_i}\Gamma_{I\to j+k}|\phi_{m_i}^{j_i}\rangle\tau_i(s_i)\langle\bar{\phi}_{m_i}^{j_i}|\Gamma_{I\to j+k}^{\dagger}\ , \tag{7}$$

where s_i, j_i, and m_i, are the invariant mass squared, spin, and helicity of the isobar. $\phi_{m_i}^{j_i}$ are isobar spinors of mass $\sqrt{s_i}$, and $\Gamma_{I\to j+k}$ is the vertex that couples the isobar I to particles j and k. In general one can have more than one isobar corresponding to the various spin and isospin channels of the two-body subsystem that are kept. The on-shell T matrix is given by the matrix elements of Eq. (7) between on-shell spinors for the two initial and the two final particles. In the c.m. system this is

$$t_i^{\nu_j'\nu_k',\nu_j\nu_k}(\mathbf{p}_i',\mathbf{p}_i;s_i)=\sum_{m_i=-j_i}^{j_i}\langle\bar{u}_{\nu_j'}^{\sigma_j}(\mathbf{p}_i')\bar{u}_{\nu_k'}^{\sigma_k}(-\mathbf{p}_i')|\Gamma_{I\to j+k}|\phi_{m_i}^{j_i}(\mathbf{0})\rangle\tau_i(s_i)\langle\bar{\phi}_{m_i}^{j_i}(\mathbf{0})|\Gamma_{I\to j+k}^{\dagger}|u_{\nu_j}^{\sigma_j}(\mathbf{p}_i)u_{\nu_k}^{\sigma_k}(-\mathbf{p}_i)\rangle\ . \tag{8}$$

where σ_j and ν_j are the spin and helicity of particle j. The general form of the vertex is

$$\langle\bar{\phi}_{m_i}^{j_i}(\mathbf{0})|\Gamma_{I\to j+k}^{\dagger}|u_{\nu_j}^{\sigma_j}(\mathbf{p}_i)u_{\nu_k}^{\sigma_k}(-\mathbf{p}_i)\rangle$$
$$=b_{j_i}^{\nu_j\nu_k}(p_i)\sqrt{2j_i+1}\,e^{-m_i\phi_i}d_{m_i,\nu_j-\nu_k}^{j_i}(\theta_i)\ , \tag{9}$$

with $p_i=|\mathbf{p}_i|$, and θ_i, ϕ_i the corresponding directions, while

$$b_{j_i}^{\nu_j\nu_k}(p_i)=\sum_{l_i}\left[\frac{2l_i+1}{2j_i+1}\right]^{1/2}C_{0,\nu_j-\nu_k}^{l_iS_ij_i}C_{\nu_j,-\nu_k}^{\sigma_j\sigma_kS_i}g_i^{l_i}(p_i)\ , \tag{10}$$

where l_i and S_i are the orbital angular momentum and total spin of the pair jk. In the case of uncoupled waves (πN subsystem) l_i has only one value while in the case of coupled waves (NN subsystem) l_i can have two values. The functions $g_i^{l_i}(p_i)$ are form factors that will be specified later. The normalization of the two-body amplitudes is such that in the case of uncoupled waves the functions $\tau_i(s_i)$ are given in terms of the phase shifts by

$$\tau_i(s_i)=-\frac{4\sqrt{s_i}}{\pi p_i[g_i^{l_i}(p_i)]^2}e^{i\delta(s_i)}\sin\delta(s_i)\ . \tag{11}$$

Thus, for the πN subsystem we constructed the amplitudes $\tau_i(s_i)$ using directly the experimental πN phase shifts in the physical region $s_i\geq(M+\mu)^2$, and the partial-wave amplitudes deduced from fixed-t dispersion relations [21] and crossing symmetry [22] in the unphysical region $0<s_i<(M+\mu)^2$. If we substitute the isobar ansatz (7) into the integral equations (1) and define new amplitudes F_{i1} as (here to simplify the notation we suppress the helicity index m_i)

$$T_i|\phi_d\rangle=\Gamma_{I\to j+k}|\phi^{j_i}\rangle\tau_i(s_i)F_{i1}\ , \tag{12}$$

where ϕ_d is the initial deuteron wave function, then the amplitudes F_{i1} obey the quasi-two-body equations [19]

$$F_{i1}=(1-\delta_{i1})V_{i1}+\sum_{j\neq i}V_{ij}\tau_jF_{j1}\ , \tag{13}$$

where

$$V_{ij}=\Gamma_{I\to j+k}^{\dagger}G_k\Gamma_{J\to k+i}\ . \tag{14}$$

The transition potentials (14) can be of two kinds. Either a pion is exchanged between two πN isobars or a nucleon is exchanged between a πN and a NN isobar. We show these two possibilities in Fig. 1, where Δ denotes a πN isobar and d denotes a NN isobar. Since in this theory all the spectator particles are required to be on-mass-shell, the space and spin dependence of the transition potentials V_{ij} is obtained by taking the matrix elements of Eq. (14) between spinors for the four external particles of Fig. 1 (actually two particles and two quasiparticles).

The $\Delta\to\pi N$ vertices that appear in Eq. (14) and Fig. 1, are given by

$$\Gamma=a(p_i),\quad\text{for the } S_{11}\text{ and } S_{31}\text{ channels}\ , \tag{15a}$$

$$\Gamma=b(p_i)\not{q}\gamma_5,\quad\text{for the } P_{11}\text{ and } P_{31}\text{ channels}\ , \tag{15b}$$

$$\Gamma_\mu=c(p_i)q_\mu,\quad\text{for the } P_{33}\text{ and } P_{13}\text{ channels}\ . \tag{15c}$$

q_μ in Eqs. (15) is the pion's four-momentum, while p_i is the magnitude of the pion-nucleon relative three-momentum in the c.m. frame of the pair (which is a Lorentz invariant [19]). The functions a, b, and c, are chosen such that the form factors $g_i^{l_i}(p_i)$ in Eq. (10) become

$$g_i^{l_i}(p_i)=\frac{p_i^{l_i}}{\Lambda^2+p_i^2}\ , \tag{16}$$

with

$$\Lambda=1\ \text{GeV}/c\ . \tag{17}$$

The spinors of the πN isobars are spin-$\frac{1}{2}$ Dirac spinors

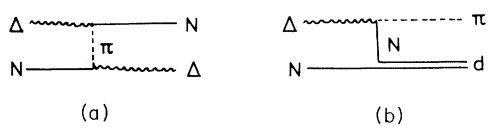

FIG. 1. Transition potentials of the πNN system. (a) Transition from a πN isobar (denoted as Δ) to another πN isobar by means of pion exchange. (b) Transition from a NN isobar (denoted as d) to a πN isobar by means of nucleon exchange.

for the S_{11}, S_{31}, P_{11}, and P_{31} channels and spin-$\frac{3}{2}$ Rarita-Schwinger spinors W^{μ} for the P_{33} and P_{13} channels.

In order to include the coupling to the NN states the amplitude $\tau_i(s_i)$ corresponding to the pion-nucleon P_{11} channel is decomposed into pole and nonpole parts [19] such that the pole part can be identified as a nucleon propagator multiplied by the square of the pion-nucleon coupling constant. Then, the transition potentials connecting to the pole part of the P_{11} amplitude are the ones describing the pion-absorption process; that is, they correspond to the transitions $\pi d \to NN$, $N\Delta \to NN$, and $NN \to NN$ (Δ is used from now on to denote any πN isobar other than the pole part of the P_{11} isobar). Since both the pole and nonpole parts of the P_{11} channel are small [19], the effect of pion absorption on the elastic and breakup channels is not very large. Notice from Eq. (15b) that our $N\Delta \to NN$ and $NN \to NN$ one pion exchange (OPE) potentials are defined with pseudovector πNN coupling.

In the transition potentials depicted by Fig. 1(b) we also need the vertex $\Gamma_{d \to NN}$ (here d denotes any NN isobar). Since we take into account only the $^1S_0$ and $^3S_1$-$^3D_1$ nucleon-nucleon channels, the corresponding vertices are [23–25]

$$\Gamma_{\mu}=\gamma_{\mu}A(p_i)-q_{\mu}B(p_i)+\frac{\not q-M}{2M}[\gamma_{\mu}D(p_i)-q_{\mu}E(p_i)] \tag{18}$$

for the $^3S_1$-$^3D_1$ channel and

$$\Gamma=\gamma_5 C(p_i)+\frac{\not q-M}{2M}\gamma_5 F(p_i) \tag{19}$$

for the $^1S_0$ channel. q_{μ} is the four-momentum of the exchanged nucleon, p_i is the magnitude of the nucleon-nucleon relative three-momentum in the c.m. frame of the pair (which is a Lorentz invariant [19]), and the functions A, B, C, D, E, and F, are form factors that will be discussed later. The isobar spinors are spin-1 spinors ϵ^{μ} in the case of the $^3S_1$-$^3D_1$ channel and 1 in the case of the $^1S_0$ channel.

The exchanged particles in Figs. 1(a) and 1(b) are off-mass-shell and they are represented by the propagator G_k in Eq. (14). The propagator of the exchanged pion in Fig. 1(a) is given by

$$G_k=\frac{1}{q_0^2-\mathbf{q}^2-\mu^2}=\frac{1}{2\omega(\mathbf{q})}\left[\frac{1}{q_0-\omega(\mathbf{q})}-\frac{1}{q_0+\omega(\mathbf{q})}\right], \tag{20}$$

where $\omega(\mathbf{q})=\sqrt{\mathbf{q}^2+\mu^2}$, and we have decomposed the propagator into its two possible time orderings. The propagator of the exchanged nucleon in Fig. 1(b) can also be decomposed into its two possible time orderings as

$$G_k=\frac{\not q+M}{q_0^2-\mathbf{q}^2-M^2}=\frac{\not q+M}{q_0^2-E^2(\mathbf{q})}=\frac{M}{E(\mathbf{q})}\left[\frac{1}{q_0-E(\mathbf{q})}\sum_{\lambda}u_{\lambda}(\mathbf{q})\bar{u}_{\lambda}(\mathbf{q})+\frac{1}{q_0+E(\mathbf{q})}\sum_{\lambda}v_{\lambda}(-\mathbf{q})\bar{v}_{\lambda}(-\mathbf{q})\right], \tag{21}$$

where $E(\mathbf{q})=\sqrt{\mathbf{q}^2+M^2}$, u_{λ} are positive-energy spinors of mass M and helicity λ, and v_{λ} are the corresponding negative-energy spinors [Eq. (21) can be easily checked by explicitly constructing both sides using the Dirac γ matrices and spinors as shown in Appendix A]. If we use Eqs. (14) and (20) to evaluate, for example, the on-shell $NN \to NN$ transition amplitude in the c.m. system, we have that $q_0=0$ and consequently each time ordering contributes exactly $\frac{1}{2}$ of the total OPE amplitude. Thus, it is very important in this case to keep both time orderings in Eq. (20). For the $NN \to N\Delta$ and $N\Delta \to N\Delta$ transition amplitudes, we have $q_0 \neq 0$ for physical deltas (that is when the mass of the isobar is larger than $M+\mu$); however, since the nucleon and delta masses are not so different, it is also important to keep both time orderings. If, on the other hand, we use Eqs. (14) and (21) to calculate the on-shell $\pi d \to N\Delta$ transition amplitude depicted in Fig. 1(b), then $q_0 \approx M$ and the second term in Eq. (21) is much smaller than the first. Thus, there is no compelling reason in this case to keep the second term in Eq. (21), and therefore we will drop it. That is, we approximate the nucleon propagator as

$$G_k \approx \frac{M}{E(\mathbf{q})}\frac{1}{q_0-E(\mathbf{q})}\sum_{\lambda}u_{\lambda}(\mathbf{q})\bar{u}_{\lambda}(\mathbf{q}) . \tag{22}$$

In the transition potentials (14) corresponding to Fig. 1(b), both the nucleon propagator and the dNN vertex enter; therefore, due to the fact that

$$\bar{u}_{\lambda}(\mathbf{q})\frac{\not q-M}{2M}=\frac{\not q-M}{2M}u_{\lambda}(\mathbf{q})=0 , \tag{23}$$

the form factors $D(p_i)$ and $E(p_i)$ in Eq. (18) and $F(p_i)$ in Eq. (19) do not contribute. That is, the dNN vertices become effectively

$$\Gamma^{\mu}=\gamma_{\mu}A(p_i)-q_{\mu}B(p_i), \quad \text{for the } ^3S_1\text{-}^3D_1 \text{ channel} , \tag{24a}$$

$$\Gamma=\gamma_5 C(p_i), \quad \text{for the } ^1S_0 \text{ channel} , \tag{24b}$$

as a consequence of the approximation (22). If the NN isobar in Fig. 1(b) is a physical deuteron (i.e., its invariant mass is equal to the mass of the deuteron), the form factors A and B can be related to the S- and D-wave components of the deuteron wave function as [19,25] [notice that due to a misprint the form factors A and B were interchanged in Eq. (78) of Ref. [19]]

$$A(p_i)=\lambda[m_d-2E(p_i)]\left[\psi_0(p_i)+\frac{1}{\sqrt{2}}\psi_2(p_i)\right], \tag{25}$$

$$B(p_i)=\lambda[m_d-2E(p_i)]\left[\frac{E(p_i)-M}{p_i^2}\psi_0(p_i) - \frac{2E(p_i)+M}{\sqrt{2}p_i^2}\psi_2(p_i)\right], \quad (26)$$

$$p_i^2=(m_d^2+M^2-q^2)^2/4m_d^2-M^2 , \quad (27)$$

$$E(p_i)=\sqrt{M^2+p_i^2} , \quad (28)$$

where λ is a constant, q^2 is the four-momentum squared of the off-shell nucleon, and m_d is the mass of the deuteron. If the mass of the NN isobar is not equal to m_d, then the form factors A and B are taken also as (25) and (26) except that now

$$p_i^2=(s_i+M^2-q^2)^2/4s_i-M^2 , \quad (29)$$

where s_i is the invariant mass squared of the isobar. Notice that if both nucleons are on-mass-shell then $q^2=M^2$ and Eq. (29) gives $p_i^2=s_i/4-M^2$ as expected.

We have introduced the approximation (22) in order to simplify the structure of the dNN vertex. A more complete treatment taking into account both terms of the propagator (21) would require also the inclusion of the form factors D and E in Eq. (18). In order to determine all four form factors that enter into Eq. (18) one would have to use a model which takes into account the negative-energy components of the deuteron wave function ($^3P_1$ and $^1P_1$ components) such as, for example, the model proposed by Buck and Gross [25].

The form factor C of the $^1S_0$ channel can formally be related to the wave function of the $^1S_0$ antibound state similarly as Eqs. (25) and (26), or equivalently

$$C(p_i)=\lambda t_0(p_i,p_i'=0;E=0) , \quad (30)$$

where $t_0(p_i,0;0)$ is the nonrelativistic half-off-shell T matrix of the $^1S_0$ channel with p_i given by Eq. (29). We used for the wave functions ψ_0, ψ_2, and the half-shell T matrix t_0, the solutions of the Paris potential [27].

The functions $\tau_i(s_i)$ for the NN isobars were obtained by requiring (a) that they satisfy the normalization condition (11), and (b) that the wave function of the NN scattering states be orthogonal to the NN bound state. The orthogonality property, as we will see when we give the results, is very important for the breakup reactions. If we use Eqs. (9) and (10) to calculate the form factors $g_i^{l_i}(p_i)$ by taking matrix elements of $\Gamma_{d\to NN}$ between spinors for the isobar and nucleons (the correct prescription in this case [23–25] is to use $\bar{u}_2\Gamma v_1$ for the $^1S_0$ channel and $\bar{u}_2\epsilon^\mu\Gamma_\mu v_1$ for the $^3S_1$-$^3D_1$ channel, where u_2 is a spinor for nucleon 2, v_1 is a charge-conjugated spinor for nucleon 1, and ϵ^μ is a spin-1 spinor for the NN isobar) we get

$$g_i^{l_i}(p_i)=\lambda\frac{\sqrt{2}E(p_i)}{M}[m_d-2E(p_i)]\psi_{l_i}(p_i) , \quad l_i=0,2 , \quad (31)$$

for the $^3S_1$-$^3D_1$ channel and

$$g_i^0(p_i)=\lambda\frac{\sqrt{2}E(p_i)}{M}[m_d-2E(p_i)]t_0(p_i,p_i'=0;E=0) , \quad (32)$$

for the $^1S_0$ channel. We obtained therefore

$$\tau_i^{-1}(s_i)=1-\int_0^\infty\frac{p_i^2dp_i}{2E(p_i)}\sum_{l_i}[g_i^{l_i}(p_i)]^2\frac{1}{4E(p_i)}\frac{1}{q_0-E(p_i)+i\epsilon} , \quad (33)$$

with

$$q_0=\frac{\sqrt{s_i}}{2} . \quad (34)$$

In the case of the $^3S_1$-$^3D_1$ channel, the parameter λ was chosen such that $\tau_i(s_i)$ has a pole at $s_i=m_d^2$, while in the case of the $^1S_0$ channel it was chosen such that $\tau_i(s_i)$ has an antibound state at $s_i=m_a^2$. Notice that in the nonrelativistic limit Eq. (33) would correspond to the unitary pole or PEST1 approximation [28].

The integral equations (13) are written in explicit form as

$$F_{i1,JT}^{\alpha_i,\alpha_1}(k_i,k_1)=(1-\delta_{i1})V_{i1,JT}^{\alpha_i,\alpha_1}(k_i,k_1)+\sum_{j\neq i}\sum_{\alpha_j}\int_0^{k_j^{\max}}\frac{k_j^2dk_j}{2\omega_j}V_{ij,JT}^{\alpha_i,\alpha_j}(k_i,k_j)\tau_{\alpha_j}(s_j)F_{j1,JT}^{\alpha_j,\alpha_1}(k_j,k_1) , \quad (35)$$

with

$$k_j^{\max}=\left[\frac{(S+M_j^2)^2}{4S}-M_j^2\right]^{1/2} , \quad (36)$$

$$s_j=(\sqrt{S}-\omega_j)^2-k_j^2 , \quad (37)$$

$$\omega_j=\sqrt{k_j^2+M_j^2} , \quad (38)$$

where S, J, and T are the invariant mass squared, total angular momentum, and total isospin of the system, while M_j and k_j are the mass and the magnitude of the three-momentum of particle j in the three-body c.m. frame.

$k_j^{\max}$ corresponds to the value of k_j for which $s_j=0$ in Eq. (37) [20]. The discrete quantum numbers α_i are

$$\alpha_i=\{l_i S_i t_i j_i m_i \nu_i\} , \tag{39}$$

where l_i, S_i, t_i, and j_i, are the orbital angular momentum, spin, isospin, and total angular momentum of the pair jk, while m_i and ν_i are the helicity of the pair jk, that is, the magnetic projection of $\mathbf{j}_i$ along the direction $\mathbf{k}_j+\mathbf{k}_k$ and the helicity of particle i. The transition potentials $V_{ij,JT}^{\alpha_i,\alpha_j}(k_i,k_j)$ in Eq. (35) are obtained by partial-wave projecting the expression (14). The input of the integral equations (35), as already mentioned, consists of the six S- and P-wave pion-nucleon channels (S_{11}, S_{31}, P_{11}, P_{13}, P_{31}, and P_{33}) and the nucleon-nucleon $^1S_0$ and $^3S_1$-$^3D_1$ channels.

B. The πd breakup amplitude

The amplitude for the πd breakup process is obtained from the solution of the integral equations described in the previous section as

$$A_{M_0}^{\mu_1\mu_2\mu_3}(\mathbf{k}_1',\mathbf{k}_2,\mathbf{k}_3;\mathbf{Q}_0)=\sum_{i=1}^{3}\sum_{\beta_i}\langle p_i k_i;\beta_i|T_i|k_1;M_0\rangle\mathcal{Y}_{\beta_i,M_0}^{\mu_i\mu_j\mu_k}(\hat{p}_i,\hat{k}_i) , \tag{40}$$

where due to energy and momentum conservation only five continuous variables are independent in the final state. $\mathbf{Q}_0=\hat{\mathbf{z}}k_1$ is the initial momentum of the deuteron and M_0 its spin projection (which is identical to the helicity since the deuteron is moving in the positive z direction), while $\mathbf{k}_1'$, $\mathbf{k}_2$, $\mathbf{k}_3$ are the final momenta of the three particles and μ_1,μ_2,μ_3 their spin projections. $\mathbf{p}_i$ is the relative momentum of the pair jk measured in the c.m. frame of the pair. The discrete quantum numbers are

$$\beta_i=\{l_i S_i t_i j_i L_i Z_i JT\} , \tag{41}$$

and the matrix elements and angular functions in Eq. (40) are given by

$$\langle p_i k_i;\beta_i|T_i|k_1;M_0\rangle=\sum_{m_i\nu_i}\sqrt{(2L_i+1)/(2J+1)}C_{m_i,-\nu_i,0}^{Z_i,L_i,J}C_{m_i,-\nu_i}^{j_i\sigma_i Z_i}2\sqrt{2\omega_d(k_1)}g_{l_i}(p_i)\tau_{\alpha_i}(s_i)F_{i1,JT}^{\alpha_i,\alpha_1}(k_i,k_1) , \tag{42}$$

$$\mathcal{Y}_{\beta_i,M_0}^{\mu_i\mu_j\mu_k}(\hat{p}_i,\hat{k}_i)=C_{\nu_j+\nu_k,\nu_i}^{t_i\tau_i T}C_{\nu_j,\nu_k}^{\tau_j\tau_k t_i}\sum_{\eta_i}C_{\eta_i+\mu_i,M_0-\eta_i-\mu_i}^{Z_i L_i J}C_{\eta_i,\mu_i}^{j_i\sigma_i Z_i}C_{\eta_i-\mu_j-\mu_k,\mu_j+\mu_k}^{l_i S_i j_i}C_{\mu_j,\mu_k}^{\sigma_j\sigma_k S_i}Y_{l_i,\eta_i-\mu_j-\mu_k}(\hat{p}_i)Y_{L_i,M_0-\eta_i-\mu_i}(\hat{k}_i) , \tag{43}$$

where $\omega_d(k_1)=\sqrt{m_d^2+k_1^2}$ with m_d being the mass of the deuteron. $\sigma_i,\sigma_j,\sigma_k$ are the spins and τ_i,τ_j,τ_k the isospins of the three particles. L_i is the orbital angular momentum between particle i and the pair j,k, and Z_i is the total effective spin between particle i and the pair j,k. $g_{l_i}(p_i)$ are the form factors defined by Eqs. (9) and (10).

Since we have assumed particle 1 to be the pion and particles 2 and 3 the two nucleons which are identical particles, the basis states of the expansion (40)–(43) will be chosen of the form

$$|1\rangle=|ijk=123\rangle , \tag{44a}$$

$$|2\rangle=|ijk=231\rangle , \tag{44b}$$

$$|3\rangle=|ijk=321\rangle , \tag{44c}$$

which means that

$$|3\rangle=P_{23}|2\rangle , \tag{45}$$

where P_{23} is the permutation operator of particles 2 and 3. Then, the Pauli principle requires that

$$F_{31,JT}^{\alpha_3,\alpha_1}(k_3,k_1)=-F_{21,JT}^{\alpha_2,\alpha_1}(k_2,k_1) ,$$
$$\text{if } \alpha_2=\alpha_3 \text{ and } k_2=k_3 . \tag{46}$$

Since the amplitude $F_{11,JT}^{\alpha_1',\alpha_1}(k_1',k_1)$ results from having a nucleon-nucleon interaction in the final state, the quantum numbers α_1' that enter there are only those allowed by the Pauli principle. Thus, the full breakup amplitude (40) which involves all three amplitudes is guaranteed to satisfy the Pauli principle.

The expansion of the final three-body state in Eqs. (40)–(43) does not correspond to helicity states but to the standard choice where the spins of the three particles refer to a fixed set of axes. This does not mean, however, that they are nonrelativistic states, since the momenta $\mathbf{p}_i$ and $\mathbf{k}_i$ are calculated with exact relativistic kinematics. Only the treatment of the spin is at this stage not fully relativistic. Due to the discontinuities of the helicity states [29,30], we have found that the expansion in terms of three-body helicity states [30,31,6] becomes problematic when the three particles do not lie in a plane with the incident momentum. Thus, the three-body states of Eqs. (40)–(43) do not take into account the "Wigner rotation of the spin in a Lorenz transformation" which is a relativistic effect [30] due to the fact that in a velocity diagram the sum of the internal angles of a triangle is less

than π. This effect, however, is quite small as we have checked in the case when the three particles lie in a plane with the incident momentum. For example, at 256 MeV incident pion energy, the kinematically complete differential cross section changes by less than 1% due to the Wigner rotation of the spin. The effects are consequently smaller in the case of the inclusive reactions.

C. The inclusive πd breakup observables

In order to calculate the differential cross section and initial-state polarization observables in the case of the kinematically complete reaction, one needs the fivefold trace and initial deuteron density matrix defined respectively as

$$\rho^{(5)}(k_i,\theta_{k_i},\phi_{k_i},\theta_{p_i},\phi_{p_i})=\sum_{M_0\mu_1\mu_2\mu_3}|A^{\mu_1\mu_2\mu_3}_{M_0}(\mathbf{k}'_1,\mathbf{k}_2,\mathbf{k}_3;\mathbf{Q}_0)|^2 , \tag{47}$$

$$\rho^{(5)}_{M_0M'_0}(k_i,\theta_{k_i},\phi_{k_i},\theta_{p_i},\phi_{p_i})=\sum_{\mu_1\mu_2\mu_3}A^{\mu_1\mu_2\mu_3*}_{M_0}(\mathbf{k}'_1,\mathbf{k}_2,\mathbf{k}_3;\mathbf{Q}_0)A^{\mu_1\mu_2\mu_3}_{M'_0}(\mathbf{k}'_1,\mathbf{k}_2,\mathbf{k}_3;\mathbf{Q}_0) . \tag{48}$$

The kinematically complete observables are then given by [32]

$$\frac{d^3\sigma}{dk_i d\Omega_{k_i}d\Omega_{p_i}}=\frac{\pi^4k_i^2p_i}{6k_1\sqrt{S(M_i^2+k_i^2)(M_i^2+p_i^2)}}\rho^{(5)}(k_i,\theta_{k_i},\phi_{k_i},\theta_{p_i},\phi_{p_i}) , \tag{49}$$

$$T^{(5)}_{LM}=\sum_{M_0M'_0}\sqrt{3}(-1)^{1-M_0}C^{11L}_{M'_0,-M_0,M}\frac{\rho^{(5)}_{M_0M'_0}(k_i,\theta_{k_i},\phi_{k_i},\theta_{p_i},\phi_{p_i})}{\rho^{(5)}(k_i,\theta_{k_i},\phi_{k_i},\theta_{p_i},\phi_{p_i})} . \tag{50}$$

where in Eq. (49) the magnitude of the relative momentum p_i is determined by k_i and the invariant mass squared S as

$$p_i^2=\frac{[s_i-(M_j+M_k)^2][s_i-(M_j-M_k)^2]}{4s_i} , \tag{51}$$

$$s_i=S+M_i^2-2\sqrt{S(M_i^2+k_i^2)} . \tag{52}$$

In order to calculate the inclusive observables one needs the threefold trace and initial-state density matrix which can be obtained from those of Eqs. (47) and (48) as

$$\rho^{(3)}(k_i,\theta_{k_i},\phi_{k_i})=\int d\Omega_{p_i}\rho^{(5)}(k_i,\theta_{k_i},\phi_{k_i},\theta_{p_i},\phi_{p_i}) , \tag{53}$$

$$\rho^{(3)}_{M_0M'_0}(k_i,\theta_{k_i},\phi_{k_i})=\int d\Omega_{p_i}\rho^{(5)}_{M_0M'_0}(k_i,\theta_{k_i},\phi_{k_i},\theta_{p_i},\phi_{p_i}) . \tag{54}$$

The inclusive differential cross section and initial-state polarization observables are then given by

$$\frac{d^2\sigma}{dk_i d\Omega_{k_i}}=\frac{\pi^4k_i^2p_i}{6k_1\sqrt{S(M_i^2+k_i^2)(M_i^2+p_i^2)}}\rho^{(3)}(k_i,\theta_{k_i},\phi_{k_i}) , \tag{55}$$

$$T^{(3)}_{LM}=\sum_{M_0M'_0}\sqrt{3}(-1)^{1-M_0}C^{11L}_{M'_0,-M_0,M}\frac{\rho^{(3)}_{M_0M'_0}(k_i,\theta_{k_i},\phi_{k_i})}{\rho^{(3)}(k_i,\theta_{k_i},\phi_{k_i})} . \tag{56}$$

III. RESULTS

Data on inclusive πd breakup reactions are naturally divided into two sets, depending on whether a pion or a nucleon is detected. If a pion is detected, one can have the normal breakup reactions $^2\mathrm{H}(\pi^\pm,\pi^\pm)X$ where $X=pn$, or a charge exchange process $^2\mathrm{H}(\pi^\pm,\pi^0)X$, where X represents either two protons or two neutrons depending on the charge of the incident pion. If a nucleon is detected, one can have either a pure breakup reaction like $^2\mathrm{H}(\pi^+,n)X$ and $^2\mathrm{H}(\pi^-,p)X$, where $X=\pi^+p$ and $X=\pi^-n$, respectively, or a mixture of breakup and charge exchange like $^2\mathrm{H}(\pi^+,p)X$ and $^2\mathrm{H}(\pi^-,n)X$, where in the first case $X=\pi^+n$ or $X=\pi^0p$, and in the second case $X=\pi^-p$ or $X=\pi^0n$.

We will calculate the differential cross sections for all the existing data where a pion or a nucleon is detected and we will present predictions where no data exist. We will, however, exclude any comparison to older bubble-chamber data [13–15], since nowadays this is an outdated experimental technique [33] and in our opinion those data should be remeasured.

A. Pion detection data

The reaction $^2\mathrm{H}(\pi^+\pi^+)X$ has been measured recently by Khandaker *et al.* [18], for an incident pion energy of 96.5 MeV. We show in Fig. 2 the differential cross section $d\sigma/d\Omega$ of Khandaker *et al.* [18] and compare it with our theoretical results. The dashed line is the impulse approximation, while the dot-dashed line is the distorted-wave impulse approximation, and the solid line refers to the full calculation. The result of the full calculation when we use the Bonn deuteron wave function [34]

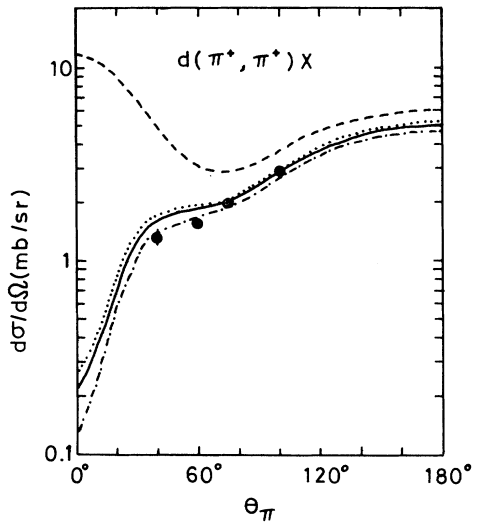

FIG. 2. Differential cross section of the inelastic reaction $^2H(\pi^+,\pi^+)X$ at 96.5 MeV. The dashed line is the result of the impulse approximation, the dot-dashed line the result of the distorted-wave impulse approximation, the solid line the result of the full calculation, and the dotted line the result of the full calculation with the Bonn deuteron wave function. The experimental points are from Ref. [18].

instead of the usual Paris wave function [27] is shown by the dotted line. The distorted wave impulse approximation and the two full calculations describe the data reasonably well. The impulse approximation, on the other hand, disagrees strongly with the data and with the other calculations, in particular, as one approaches the forward direction. The failure of the impulse approximation is a consequence of the fact that in that approximation the wave function of the two final nucleons is not orthogonal to the deuteron wave function. In order to understand these results, let us consider the simpler case of the distorted-wave impulse approximation. We notice from Eqs. (5) and (6) that

$$\langle \mathbf{k}'_1\mathbf{p}|\, A^{\mathrm{DWIA}}|\phi_d\mathbf{k}_1\rangle = \sum_{i=2,3}\langle \mathbf{k}'_1\chi_{\mathbf{p}}^{(-)}|t_i|\phi_d\mathbf{k}_1\rangle\ , \qquad (57)$$

where $\mathbf{k}_1$ and $\mathbf{k}'_1$ are the initial and final momenta of the pion and ϕ_d is the deuteron wave function. Since the pion-nucleon amplitude t_i varies slowly in momentum space as compared with the nucleon-nucleon wave functions ϕ_d and $\chi_{\mathbf{p}}^{(-)}$, the matrix element (57) can be factorized as

$$\langle \mathbf{k}'_1\mathbf{p}|\, A^{\mathrm{DWIA}}|\phi_d\mathbf{k}_1\rangle$$

$$\approx \sum_{i=2,3}\langle \mathbf{k}'_1|t_i|\mathbf{k}_1\rangle\int d\mathbf{r}\chi_{\mathbf{p}}^{(-)}(\mathbf{r})^* e^{i(\mathbf{k}'_1-\mathbf{k}_1)\cdot\mathbf{r}}\phi_d(\mathbf{r})\ , \qquad (58)$$

therefore, since the functions $\chi_{\mathbf{p}}^{(-)}$ and ϕ_d are orthogonal to each other, one must have that

$$\langle \mathbf{k}'_1\mathbf{p}|\, A^{\mathrm{DWIA}}|\phi_d\mathbf{k}_1\rangle \to 0 \quad \text{if } \mathbf{k}'_1\to\mathbf{k}_1\ , \qquad (59)$$

so that the cross section must vanish in the forward direction $\mathbf{k}'_1=\mathbf{k}_1$. Of course, this condition is never satisfied exactly, since first of all, Eq. (58) is only an approximation, and secondly, due to the binding energy of the deuteron, the point $\mathbf{k}'_1=\mathbf{k}_1$ is never reached in the breakup process. However, as one can see in Fig. 2, the effect of orthogonality is to suppress strongly the cross section in the forward direction as compared with the impulse approximation [35]. In the case of the impulse approximation [see Eq. (3)], the distorted wave $\langle\chi_{\mathbf{p}}^{(-)}|$ in Eq. (6) has been replaced by the plane wave $\langle\mathbf{p}|$ and therefore the effect of orthogonality is destroyed. We show in Figs. 3 and 4 the corresponding results for the double differential cross section $d^2\sigma/d\Omega_\pi dE_\pi$ for the five outgoing pion angles measured by Khandaker *et al.* [18]. The small peak seen in the $\theta_\pi=40°$ spectrum at low momenta is most likely due to experimental background since none of the theoretical curves generate such a structure and also it does not show up in the remaining experimental spectra. Again as in the previous figure, the distorted-wave impulse approximation and the two full calculations describe the data reasonably well, while the impulse approximation fails badly as one approaches the forward direction.

The differential cross section of the charge-exchange reaction $^2H(\pi^-,\pi^0)X$ where $X=nn$ has been measured by Moinester *et al.* [17] for an incident pion energy of 164.1 MeV. We show these results in Fig. 5 where we

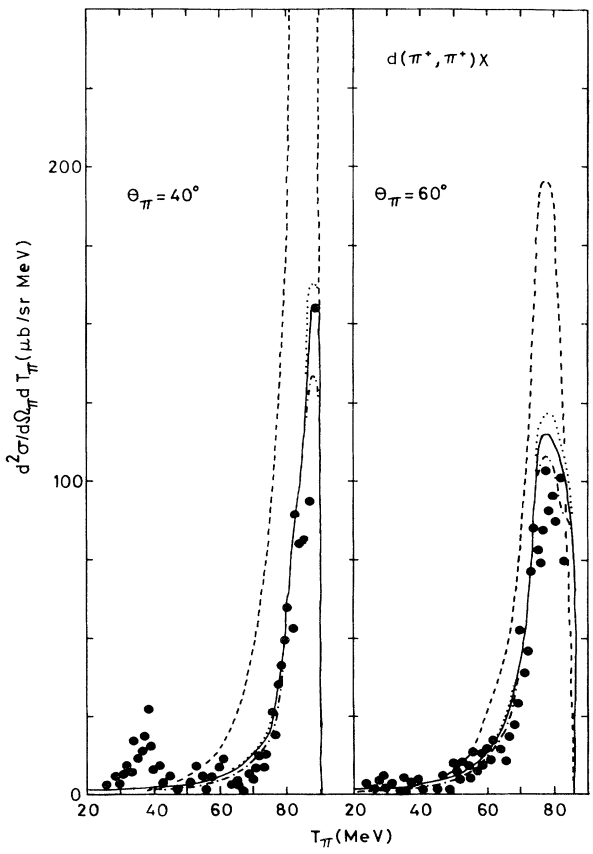

FIG. 3. Double differential cross section of the inelastic reaction $^2H(\pi^+,\pi^+)X$ at 96.5 MeV for two outgoing pion angles. The labeling of the curves and the data are as in Fig. 2.

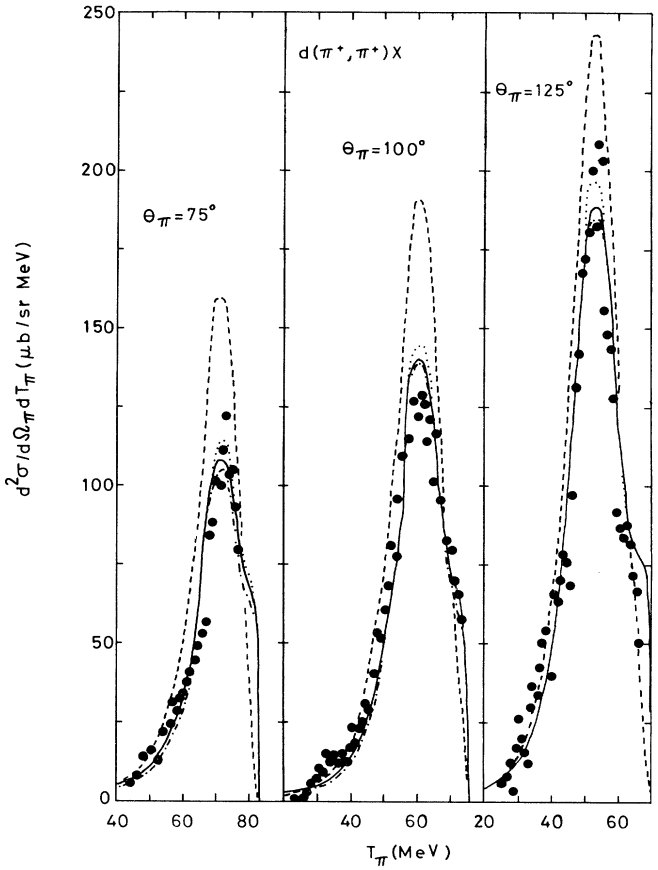

FIG. 4. Double differential cross section of the inelastic reaction ^{2}H(π^+,π^+)X at 96.5 MeV for three outgoing pion angles. The labeling of the curves and the data are as in Fig. 2.

compare them with the predictions of our model. The curve corresponding to the distorted-wave impulse approximation is not shown since it is indistinguishable from that of the impulse approximation. One should keep in mind that the condition of orthogonality has no effect here, since the final two neutrons are not allowed to be in the $^3S_1$-$^3D_1$ state. The fact that the cross section tends to vanish in the forward direction already at the level of the impulse approximation is a direct consequence of the Pauli principle as expressed by Eq. (46), since in this case the isospins of the two neutrons in the final state are equal, and therefore the amplitudes $F^{\alpha_2,\alpha_1}_{21,JT}(k_2,k_1)$ and $F^{\alpha_3,\alpha_1}_{31,JT}(k_3,k_1)$ will cancel each other if the momenta $\mathbf{k}_2$ and $\mathbf{k}_3$ are equal. At $\theta_\pi=0$, the dominant contribution to the cross section comes from the configuration $k_2=k_3=k_{\max}$ for which the cancelation of the two amplitudes is exact.

Since at the present time only the single differential cross section $d\sigma/d\Omega$ exists (the double differential cross sections of Ref. [17] are still in the process of being analyzed), we have chosen three pion angles $\theta_\pi=25°$, 75°, and 125° to present our predictions for the double differential cross section. We show these results in Fig. 6 where we have used again the impulse approximation (dashed line), the distorted-wave impulse approximation (dot-dashed line), the full calculation (solid line), and the full calculation with the Bonn deuteron wave function (dotted line). The energy at which the cross section peaks for each angle is determined by the quasifree process $\pi^-p\rightarrow\pi^0n$ with the spectator neutron being left at rest in the labora-

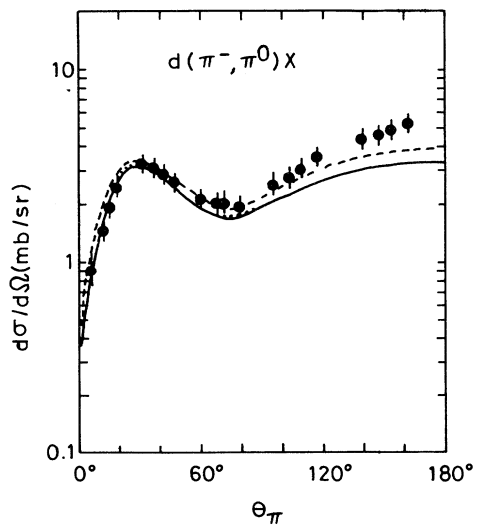

FIG. 5. Differential cross section of the reaction ^{2}H(π^-,π^0)X at 164.1 MeV. The labeling of the curves is as in Fig. 2. The experimental points are from Ref. [17].

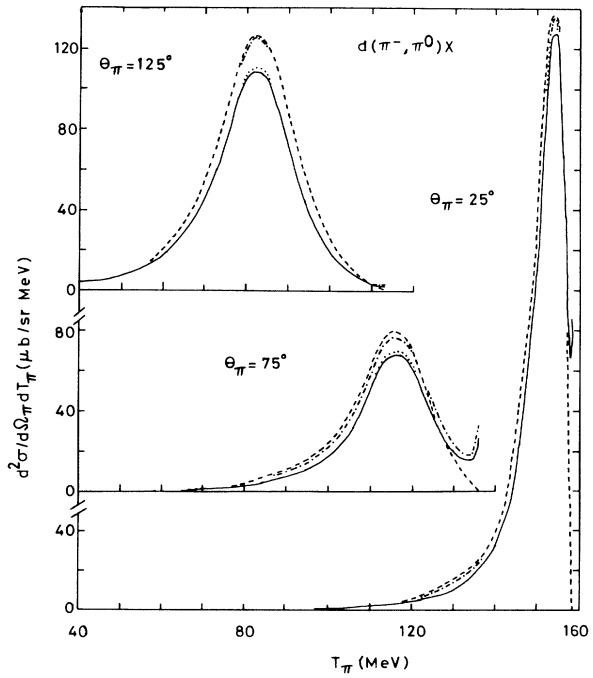

FIG. 6. Double differential cross section of the reaction ^{2}H(π^-,π^0) at 164.1 MeV for three outgoing pion angles. The labeling of the curves is as in Fig. 2.

tory system. The raising of the cross section at high pion energies for $\theta_\pi = 25°$ and 75° is the result of the final-state neutron-neutron interaction in the $^1S_0$ channel.

B. Nucleon detection data

We have calculated the predictions of our model for the reactions $^2H(\pi^-,p)X$ and $^2H(\pi^+,p)X$ [which are the isobaric analogs of the reactions $^2H(\pi^+,n)X$ and $^2H(\pi^-,n)X$, respectively] at $T_\pi = 256$ MeV. We show in Figs. 7 and 8 our predictions for the differential cross sections using the same four theoretical prescriptions as in the previous results. The main feature of these results is that while the π^- cross section stays relatively flat, the π^+ cross section falls down by almost two orders of magnitude as one goes to large angles. We will discuss next the meaning of these results.

The reaction $^2H(\pi^-,p)X$ is dominated by the single-scattering term $\pi^- n \to \pi^- n$ with the proton acting as spectator, since the contribution of the $\pi^- p \to p\pi^-$ process comes into the amplitude reduced by a factor of $\frac{1}{3}$ due to isospin (assuming delta-isobar dominance). Thus, the protons that are detected are mostly spectator protons which always tend to be produced with zero momentum and therefore they give rise to an isotropic angular distribution. We have checked that including only the $\pi^- n \to \pi^- n$ term leads to an essentially constant differential cross section of about 10 mb/sr. Thus, the small anisotropy observed in the impulse approximation result of Fig. 7 is produced by the contribution of the $\pi^- p \to p\pi^-$ term. The effect of the higher-order scattering terms is to lower the cross section and to increase somewhat the anisotropy.

The reaction $^2H(\pi^+,p)X$ is dominated by the single-scattering term $\pi^+ p \to p\pi^+$ with the neutron as spectator since the term $\pi^+ n \to \pi^+ n$ with the proton as spectator enters into the amplitude reduced by a factor of $\frac{1}{3}$. Thus,

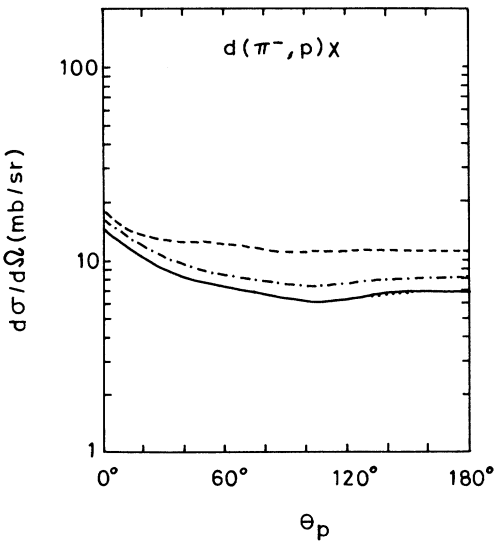

FIG. 7. Differential cross section of the reaction $^2H(\pi^-,p)X$ at 256 MeV. The labeling of the curves is as in Fig. 2.

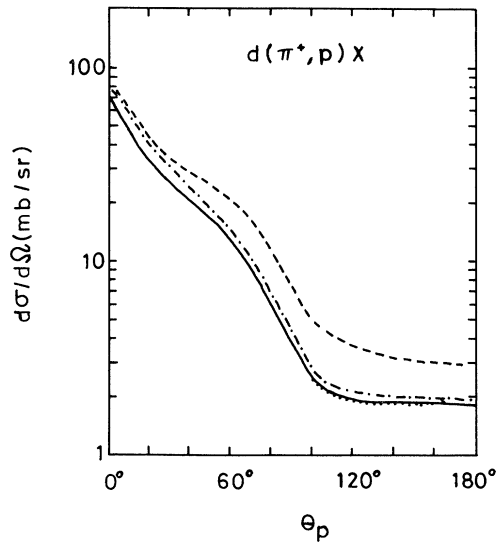

FIG. 8. Differential cross section of the reaction $^2H(\pi^+,p)X$ at 256 MeV. The labeling of the curves is as in Fig. 2.

the protons observed here are essentially those knocked out by the pion and the differential cross section follows the general shape of the free $\pi^+ p \to p\pi^+$ cross section. Since in the laboratory system the free $\pi^+ p \to p\pi^+$ cross section is zero for $\theta > 90°$, this explains the dramatic fall off of the $^2H(\pi^+,p)X$ cross section in the backward hemisphere that is observed in Fig. 8. As a matter of fact the protons observed at large angles in Fig. 8 are essentially the spectator protons connected with the process $\pi^+ n \to \pi^+ n$. Thus, ignoring the contribution of the charge-exchange reaction and assuming delta-isobar dominance implies that the cross section of the $^2H(\pi^+,p)X$ process at backward angles should be a factor of 9 smaller than the corresponding cross section of the $^2H(\pi^-,p)X$ process. The factor that we get, however, is closer to 4 as a consequence of the presence of the charge-exchange cross section and the interference of non delta-isobar contributions.

Finally, we would like to notice from the results of Figs. 7 and 8 that the full calculation lies below the impulse approximation, in some cases by as much as a factor of 2, and the results with the Paris or Bonn deuteron wave function are essentially indistinguishable.

We show in Fig. 9 the double differential cross section of the $^2H(\pi^-,p)X$ reaction at $\theta_p = 25°$. One sees clearly the two peaks at 0 and 130 MeV. The dominant peak is the one at $T_p = 0$ which is due to the spectator protons connected with the process $\pi^- n \to \pi^- n$ as mentioned before. The smaller peak at $T_p \approx 130$ MeV is produced by the knocked-out protons coming from the process $\pi^- p \to p\pi^-$ with the neutron acting as spectator. We show in Fig. 10 the corresponding double differential cross sections for the proton angles 75° and 125°. At $\theta_p = 75°$ only the peak at $T_p = 0$ due to the spectator protons is seen, although the peak from the knocked-out protons should have appeared at $T_p \approx 10$ MeV. However, this second peak is completely wiped out by the dominant

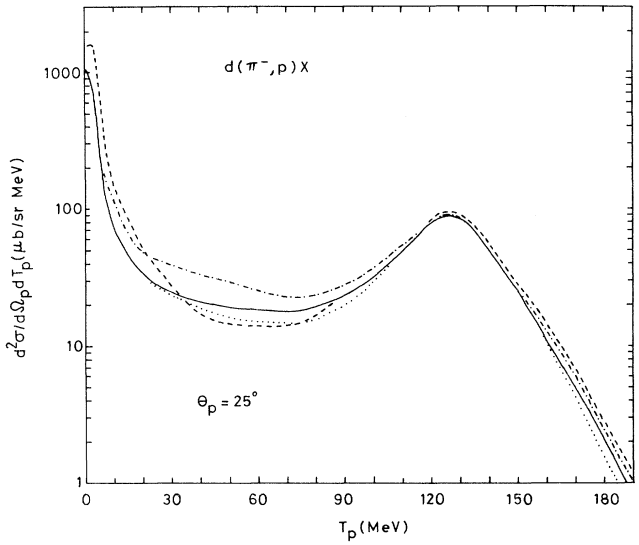

FIG. 9. Double differential cross section of the reaction ^{2}H(π^-,p)X at 256 MeV for one outgoing proton angle. The labeling of the curves is as in Fig. 2.

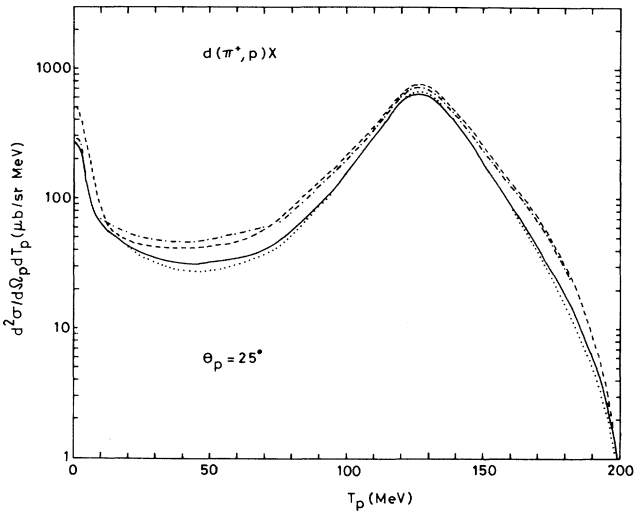

FIG. 11. Double differential cross section of the reaction ^{2}H(π^+,p)X at 256 MeV for one outgoing proton angle. The labeling of the curves is as in Fig. 2.

spectator-proton mechanism. At $\theta_p = 125°$ only the spectator protons can contribute and indeed the only peak that is seen is that at $T_p = 0$.

We show in Fig. 11 the double differential cross section of the ^{2}H(π^+,p)X reaction at $\theta_p = 25°$. Again, as in Fig. 9, one sees two peaks at 0 and 130 MeV. In this case, however, the dominant peak is the one at $T_p \approx 130$ MeV which is due to the process $\pi^+ p \rightarrow p\pi^+$ with the neutron as spectator. The peak at $T_p = 0$ due to the spectator protons connected with the process $\pi^+ n \rightarrow \pi^+ n$ is much weaker as a consequence of isospin. We show in Fig. 12 the corresponding double differential cross sections for the proton angles 75° and 125°. At $\theta_p = 75°$ one sees clearly the peak at $T_p \approx 10$ MeV due to the process $\pi^+ p \rightarrow p\pi^+$ with the neutron as spectator. At $T_p = 0$ one has a narrow peak due to the spectator mechanism plus the protons coming from the charge-exchange reaction. At $\theta_p = 125°$ there is only one peak at $T_p = 0$ from the only single-scattering process that is allowed, i.e., the spectator mechanism. However, here the full calculation gives rise to a very pronounced shoulder at $T_p \approx 50$ MeV.

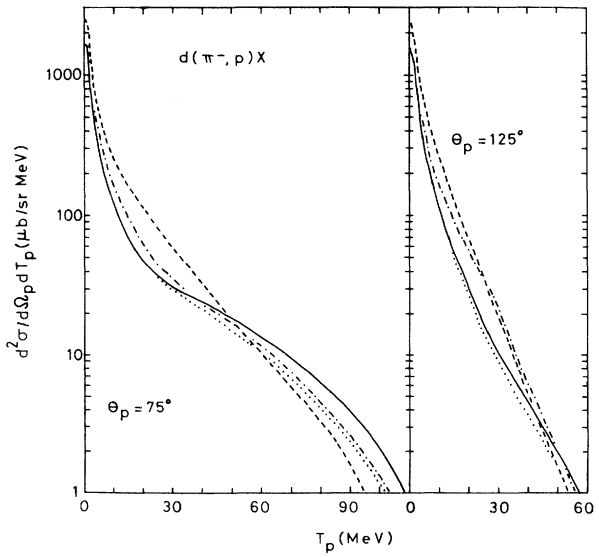

FIG. 10. Double differential cross section of the reaction ^{2}H(π^-,p)X at 256 MeV for two outgoing proton angles. The labeling of the curves is as in Fig. 2.

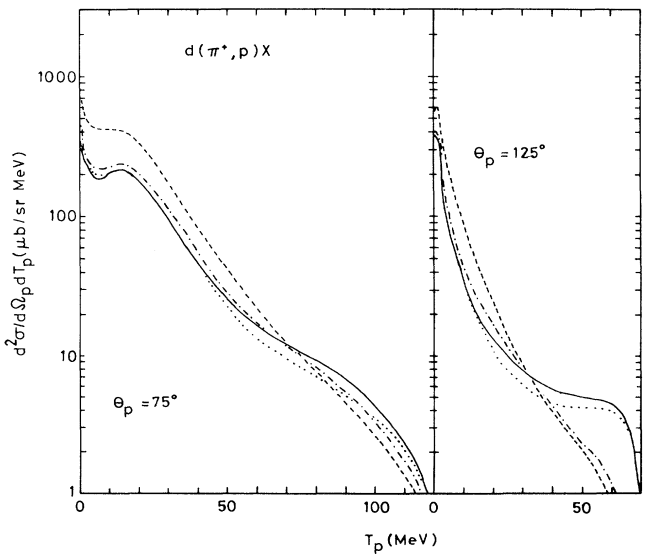

FIG. 12. Double differential cross section of the reaction ^{2}H(π^+,p)X at 256 MeV for two outgoing proton angles. The labeling of the curves is as in Fig. 2.

We have found that this shoulder is the signature of the pion-nucleon double-scattering term in which the pion scatters first on the neutron and then on the proton. Thus, in our opinion, this is a very interesting region to be studied experimentally since it provides a clean way to explore the effects of the pion-nucleon double-scattering term.

The reactions $^2H(\pi^-,p)X$ and $^2H(\pi^+,p)X$ have been measured at an angle $\theta_p = 90°$ as a function of the energy of the incident pion by Arvieux *et al.* [16], considering several fixed proton momenta. We show these data for the reaction $^2H(\pi^-,p)X$ in Fig. 13 and compare them with the predictions of our model. As one sees, the results are considerably sensitive to the deuteron wave function being used, and the predictions of the full calculation with the Bonn deuteron wave function are the ones that describe the data better. In Fig. 14 we show the corresponding results for the reaction $^2H(\pi^+,p)X$. In this case the data shows no preference for the predictions of either the Paris or Bonn deuteron wave function. However, one should keep in mind that in this case there is a third contribution to the cross section coming from the process $\pi^+ d \to \gamma pp$ which we have not taken into account (the data points at low energies where our theoretical curves give zero, are entirely due to this process). Although it has been estimated in Ref. [16] that the γpp cross section is important only at low energies, it will nevertheless have the effect of increasing somewhat the theoretical cross sections of Fig. 14. Thus, it seems likely that the Bonn deuteron wave function may at the end describe the data better. Of course, this should not be taken to indicate that the Bonn deuteron wave function is better than the Paris wave function since some additional effects like higher NN and πN partial waves, two-pion states, etc., have not been taken into account. Moreover, one would also need data on the polarization observables in order to distinguish clearly which deuteron wave function is better.

IV. FINAL REMARKS

We have performed a relativistic Faddeev calculation of inclusive πd breakup reactions at medium energies and found satisfactory agreement whenever data was available. We have studied the sensitivity of the differential cross sections to multiple scattering effects and to the use of different deuteron wave functions. The reactions $^2H(\pi,\pi)X$ are quite insensitive to which deuteron wave function is used. The reactions $^2H(\pi,N)X$, on the other hand, appear more promising for the purpose of learning about the deuteron wave function.

We were also able to isolate the various kinematical regions that are sensitive to specific multiple scattering processes. For example, the $^2H(\pi^-,p)X$ and $^2H(\pi^+,p)X$

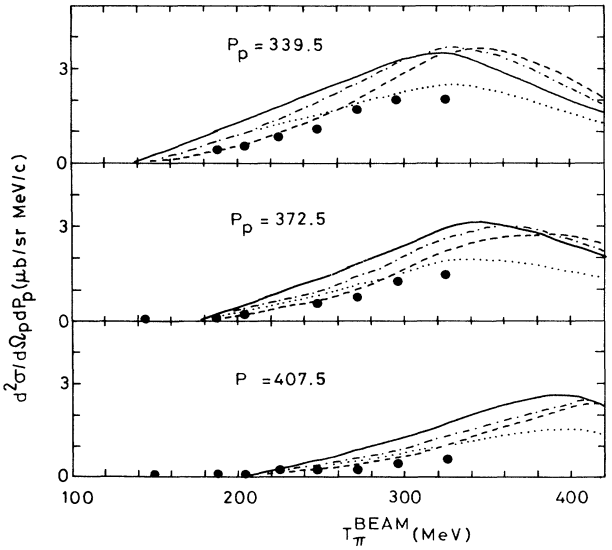

FIG. 13. Double differential cross section of the reaction $^2H(\pi^-,p)X$ at an outgoing proton angle of 90° for three values of the proton momentum (in MeV/c), as a function of the incident energy of the pion. The labeling of the curves is as in Fig. 2. The experimental points are from Ref. [16].

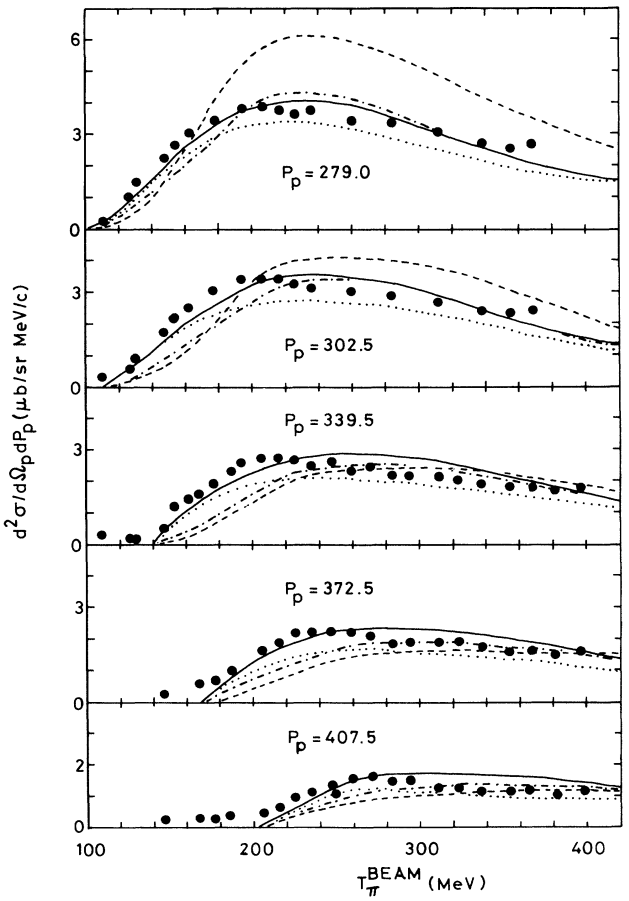

FIG. 14. Double differential cross section of the reaction $^2H(\pi^+,p)X$ at an outgoing proton angle of 90° for five values of the proton momentum (in MeV/c), as a function of the incident energy of the pion. The labeling of the curves is as in Fig. 2. The experimental points are from Ref. [16].

cross sections in the forward direction are essentially determined by the pion-nucleon single-scattering terms. A similar thing happens with the $^2H(\pi^-,\pi^0)X$ cross section where the Pauli principle also plays an important role. The reaction $^2H(\pi^+,\pi^+)X$ is determined by the pion-nucleon single-scattering term followed by a final-state nucleon-nucleon interaction. Finally, the reaction $^2H(\pi^+,p)X$ in the backward direction and for large proton momenta is dominated by the pion-nucleon double-scattering term. More experimental data on the various kinematical regions would be very helpful to isolate and study each reaction mechanism separately.

ACKNOWLEDGMENTS

We thank Prof. J. Arvieux, Prof. E. T. Boschitz, Prof. L. G. Dakhno, and Prof. G. Z. Obrant for very valuable information on the subject of this paper. This work was supported by the German Federal Ministry for Research and Technology (BMFT) under Contract No. 06 0H 754.

APPENDIX A: THE NUCLEON PROPAGATOR

We want to check that Eq. (21) is correct. Let us consider a matrix A defined as

$$A = \not{q} + M = q_0\gamma^0 - q_1\gamma^1 - q_2\gamma^2 - q_3\gamma^3 + M$$
$$= q_0\gamma^0 - q_x\gamma^1 - q_y\gamma^2 - q_z\gamma^3 + M \ . \tag{A1}$$

Using the definitions of the Dirac γ matrices given in Appendix A of Bjorken and Drell [26], we have that

$$A = q_0\begin{bmatrix}1&0&0&0\\0&1&0&0\\0&0&-1&0\\0&0&0&-1\end{bmatrix} - q_x\begin{bmatrix}0&0&0&1\\0&0&1&0\\0&-1&0&0\\-1&0&0&0\end{bmatrix} - q_y\begin{bmatrix}0&0&0&-i\\0&0&i&0\\0&i&0&0\\-i&0&0&0\end{bmatrix} - q_z\begin{bmatrix}0&0&1&0\\0&0&0&-1\\-1&0&0&0\\0&1&0&0\end{bmatrix} + M\begin{bmatrix}1&0&0&0\\0&1&0&0\\0&0&1&0\\0&0&0&1\end{bmatrix}$$
$$= \begin{bmatrix}q_0+M & 0 & -q_z & -q_x+iq_y\\ 0 & q_0+M & -q_x-iq_y & q_z\\ q_z & q_x-iq_y & -q_0+M & 0\\ q_x+iq_y & -q_z & 0 & -q_0+M\end{bmatrix} . \tag{A2}$$

The positive-energy spinors are given in Eq. (3.7) of Bjorken and Drell [26] as

$$u_+(\mathbf{q}) = \frac{1}{\sqrt{2M(M+E)}}\begin{bmatrix}M+E\\0\\q_z\\q_x+iq_y\end{bmatrix} , \tag{A3}$$

$$u_-(\mathbf{q}) = \frac{1}{\sqrt{2M(M+E)}}\begin{bmatrix}0\\M+E\\q_x-iq_y\\-q_z\end{bmatrix} , \tag{A4}$$

where

$$E = \sqrt{M^2+\mathbf{q}^2} \ . \tag{A5}$$

Then the adjoint spinors are

$$\bar{u}_+(\mathbf{q}) = u_+^\dagger(\mathbf{q})\gamma^0 = \frac{1}{\sqrt{2M(M+E)}}(M+E,0,q_z,q_x-iq_y)\begin{bmatrix}1&0&0&0\\0&1&0&0\\0&0&-1&0\\0&0&0&-1\end{bmatrix}$$
$$= \frac{1}{\sqrt{2M(M+E)}}(M+E,0,-q_z,-q_x+iq_y) , \tag{A6}$$

and

$$\bar{u}_-(\mathbf{q})=u_-^\dagger(\mathbf{q})\gamma^0=\frac{1}{\sqrt{2M(M+E)}}(0,M+E,q_x+iq_y,-q_z)\begin{bmatrix}1&0&0&0\\0&1&0&0\\0&0&-1&0\\0&0&0&-1\end{bmatrix}$$

$$=\frac{1}{\sqrt{2M(M+E)}}(0,M+E,-q_x-iq_y,q_z)\ . \tag{A7}$$

We now introduce a matrix B as

$$B=2M[u_+(\mathbf{q})\bar{u}_+(\mathbf{q})+u_-(\mathbf{q})\bar{u}_-(\mathbf{q})]\ , \tag{A8}$$

then using Eqs. (A3)–(A4) and (A6)–(A7) we have that

$$B=\frac{1}{M+E}\begin{bmatrix}M+E\\0\\q_z\\q_x+iq_y\end{bmatrix}(M+E,0,-q_z,-q_x+iq_y)+\frac{1}{M+E}\begin{bmatrix}0\\M+E\\q_x-iq_y\\-q_z\end{bmatrix}(0,M+E,-q_x-iq_y,q_z)$$

$$=\frac{1}{M+E}\begin{bmatrix}(M+E)^2&0&-(M+E)q_z&(M+E)(-q_x+iq_y)\\0&0&0&0\\q_z(M+E)&0&-q_z^2&q_z(-q_x+iq_y)\\(q_x+iq_y)(M+E)&0&-(q_x+iq_y)q_z&-q_x^2-q_y^2\end{bmatrix}$$

$$+\frac{1}{M+E}\begin{bmatrix}0&0&0&0\\0&(M+E)^2&(M+E)(-q_x-iq_y)&(M+E)q_z\\0&(q_x-iq_y)(M+E)&-q_x^2-q_y^2&(q_x-iq_y)q_z\\0&-q_z(M+E)&q_z(q_x+iq_y)&-q_z^2\end{bmatrix}$$

$$=\begin{bmatrix}M+E&0&-q_z&-q_x+iq_y\\0&M+E&-q_x-iq_y&q_z\\q_z&q_x-iq_y&-\mathbf{q}^2/(M+E)&0\\q_x+iq_y&-q_z&0&-\mathbf{q}^2/(M+E)\end{bmatrix}\ , \tag{A9}$$

so that using Eq. (A5) we get finally

$$B=\begin{bmatrix}M+E&0&-q_z&-q_x+iq_y\\0&M+E&-q_x-iq_y&q_z\\q_z&q_x-iq_y&M-E&0\\q_x+iq_y&-q_z&0&M-E\end{bmatrix}\ . \tag{A10}$$

The negative-energy spinors are given in Eq. (3.7) of Bjorken and Drell [26] as

$$v_+(\mathbf{q})=\frac{1}{\sqrt{2M(M+E)}}\begin{bmatrix}q_z\\q_x+iq_y\\M+E\\0\end{bmatrix}\ , \tag{A11}$$

$$v_-(\mathbf{q})=\frac{1}{\sqrt{2M(M+E)}}\begin{bmatrix}q_x-iq_y\\-q_z\\0\\M+E\end{bmatrix}\ , \tag{A12}$$

so that

$$v_+(-\mathbf{q})=\frac{1}{\sqrt{2M(M+E)}}\begin{pmatrix}-q_z\\-q_x-iq_y\\M+E\\0\end{pmatrix}, \tag{A13}$$

$$v_-(-\mathbf{q})=\frac{1}{\sqrt{2M(M+E)}}\begin{pmatrix}-q_x+iq_y\\q_z\\0\\M+E\end{pmatrix}. \tag{A14}$$

Then the adjoint spinors are

$$\begin{aligned}\bar{v}_+(-\mathbf{q})=v_+^\dagger(-\mathbf{q})\gamma^0&=\frac{1}{\sqrt{2M(M+E)}}(-q_z,-q_x+iq_y,M+E,0)\begin{pmatrix}1&0&0&0\\0&1&0&0\\0&0&-1&0\\0&0&0&-1\end{pmatrix}\\&=\frac{1}{\sqrt{2M(M+E)}}(-q_z,-q_x+iq_y,-M-E,0)\end{aligned} \tag{A15}$$

and

$$\begin{aligned}\bar{v}_-(-\mathbf{q})=v_-^\dagger(-\mathbf{q})\gamma^0&=\frac{1}{\sqrt{2M(M+E)}}(-q_x-iq_y,q_z,0,M+E)\begin{pmatrix}1&0&0&0\\0&1&0&0\\0&0&-1&0\\0&0&0&-1\end{pmatrix}\\&=\frac{1}{\sqrt{2M(M+E)}}(-q_x-iq_y,q_z,0,-M-E)\,.\end{aligned} \tag{A16}$$

We now introduce a matrix C as

$$C=2M[v_+(-\mathbf{q})\bar{v}_+(-\mathbf{q})+v_-(-\mathbf{q})\bar{v}_-(-\mathbf{q})]\,, \tag{A17}$$

then using Eqs. (A13)–(A16) we have that

$$\begin{aligned}C&=\frac{1}{M+E}\begin{pmatrix}-q_z\\-q_x-iq_y\\M+E\\0\end{pmatrix}(-q_z,-q_x+iq_y,-M-E,0)+\frac{1}{M+E}\begin{pmatrix}-q_x+iq_y\\q_z\\0\\M+E\end{pmatrix}(-q_x-iq_y,q_z,0,-M-E)\\&=\frac{1}{M+E}\begin{pmatrix}q_z^2&-q_z(-q_x+iq_y)&q_z(M+E)&0\\(q_x+iq_y)q_z&q_x^2+q_y^2&(q_x+iq_y)(M+E)&0\\-(M+E)q_z&(M+E)(-q_x+iq_y)&-(M+E)^2&0\\0&0&0&0\end{pmatrix}\\&\quad+\frac{1}{M+E}\begin{pmatrix}q_x^2+q_y^2&(-q_x+iq_y)q_z&0&(q_x-iq_y)(M+E)\\-q_z(q_x+iq_y)&q_z^2&0&-q_z(M+E)\\0&0&0&0\\-(M+E)(q_x+iq_y)&(M+E)q_z&0&-(M+E)^2\end{pmatrix}\\&=\begin{pmatrix}\mathbf{q}^2/(M+E)&0&q_z&q_x-iq_y\\0&\mathbf{q}^2/(M+E)&q_x+iq_y&-q_z\\-q_z&-q_x+iq_y&-M-E&0\\-q_x-iq_y&q_z&0&-M-E\end{pmatrix},\end{aligned} \tag{A18}$$

so that using Eq. (A5) we get finally

$$C=\begin{bmatrix} E-M & 0 & q_z & q_x-iq_y \\ 0 & E-M & q_x+iq_y & -q_z \\ -q_z & -q_x+iq_y & -M-E & 0 \\ -q_x-iq_y & q_z & 0 & -M-E \end{bmatrix} . \tag{A19}$$

In order to check Eq. (21), let us consider the matrix

$$\frac{1}{2E}\left[\frac{B}{q_0-E}+\frac{C}{q_0+E}\right] .$$

We first notice from Eqs. (A2), (A10), and (A19), that the off-diagonal elements of the matrices A, B, and C, satisfy

$$A_{\mu\nu}=B_{\mu\nu}=-C_{\mu\nu} , \tag{A20}$$

and therefore we have that for these elements

$$\frac{1}{2E}\left[\frac{B_{\mu\nu}}{q_0-E}+\frac{C_{\mu\nu}}{q_0+E}\right]=\frac{A_{\mu\nu}}{2E}\left[\frac{1}{q_0-E}-\frac{1}{q_0+E}\right]=\frac{A_{\mu\nu}}{q_0^2-E^2} . \tag{A21}$$

In the case of the diagonal elements, we have that

$$\frac{1}{2E}\left[\frac{B_{00}}{q_0-E}+\frac{C_{00}}{q_0+E}\right]=\frac{1}{2E}\left[\frac{M+E}{q_0-E}+\frac{E-M}{q_0+E}\right]=\frac{q_0+M}{q_0^2-E^2}=\frac{A_{00}}{q_0^2-E^2} , \tag{A22}$$

and the same holds for the element 11. Similarly,

$$\frac{1}{2E}\left[\frac{B_{22}}{q_0-E}+\frac{C_{22}}{q_0+E}\right]=\frac{1}{2E}\left[\frac{M-E}{q_0-E}+\frac{-M-E}{q_0+E}\right]=\frac{-q_0+M}{q_0^2-E^2}=\frac{A_{22}}{q_0^2-E^2} , \tag{A23}$$

and the same holds for the element 33.

Therefore, we have shown that

$$\frac{1}{2E}\left[\frac{B}{q_0-E}+\frac{C}{q_0+E}\right]=\frac{A}{q_0^2-E^2} , \tag{A24}$$

so that using Eqs. (A1), (A8), and (A17), Eq. (A24) can be rewritten as

$$\frac{M}{E}\left[\frac{1}{q_0-E}\sum_\lambda u_\lambda(\mathbf{q})\bar{u}_\lambda(\mathbf{q})+\frac{1}{q_0+E}\sum_\lambda v_\lambda(-\mathbf{q})\bar{v}_\lambda(-\mathbf{q})\right]=\frac{\not{q}+M}{q_0^2-E^2} , \tag{A25}$$

which is Eq. (21).

[1] J. H. Hoftiezer *et al.*, Phys. Lett. **88B**, 73 (1979).
[2] J. H. Hoftiezer *et al.*, Phys. Rev. C **23**, 407 (1981).
[3] H. Garcilazo, Phys. Rev. Lett. **48**, 577 (1982).
[4] A. Matsuyama, Nucl. Phys. **A379**, 415 (1982); **A386**, 624(E) (1982).
[5] E. L. Mathie, G. R. Smith, E. T. Boschitz, W. Gyles, C. R. Ottermann, S. Mango, J. A. Konter, A. Matsuyama, R. R. Johnson, and R. Olszewski, Phys. Lett. **154B**, 28 (1985).
[6] W. Gyles, E. T. Boschitz, H. Garcilazo, W. List, E. L. Mathie, C. R. Ottermann, G. R. Smith, R. Tacik, and R. R. Johnson, Phys. Rev. C **33**, 583 (1986).
[7] W. Gyles, E. T. Boschitz, H. Garcilazo, E. L. Mathie, C. R. Ottermann, G. R. Smith, S. Mango, J. A. Konter, and R. R. Johnson, Phys. Rev. C **33**, 595 (1986).
[8] W. List, E. T. Boschitz, H. Garcilazo, W. Gyles, C. R. Ottermann, R. Tacik, M. Wessler, U. Wiedner, and R. R. Johnson, Phys. Rev. C **37**, 1587 (1988).
[9] W. List, E. T. Boschitz, H. Garcilazo, W. Gyles, C. R. Ottermann, R. Tacik, S. Mango, J. A. Konter, B. van den Brandt, and G. R. Smith, Phys. Rev. C **37**, 1594 (1988).
[10] P. V. Pancella *et al.*, Phys. Rev. C **38**, 2716 (1988).
[11] E. L. Mathie *et al.*, Phys. Rev. C **41**, 193 (1990).
[12] R. Tacik, E. T. Boschitz, W. Gyles, C. R. Ottermann, M. Wessler, U. Wiedner, H. Garcilazo, and R. R. Johnson, Phys. Rev. C **30**, 1846 (1990).
[13] L. G. Dakhno, A. V. Kratsov, M. M. Makarov, V. I. Medvedev, G. Z. Obrant, V. I. Poromov, V. V. Sarantsev, G. L. Sokolov, and G. S. Sherman, Pis'ma Zh. Eksp. Teor. Fiz. **30**, 467 (1979) [JETP Lett. **30**, 436 (1979)].
[14] L. G. Dakhno, A. V. Kratsov, M. M. Makarov, V. I.

Medvedev, G. Z. Obrant, V. I. Poromov, V. V. Sarantsev, G. L. Sokolov, and G. S. Sherman, Phys. Lett. **123B**, 33 (1983).
[15] L. G. Dakhno, A. V. Kratsov, M. M. Makarov, V. I. Medvedev, G. Z. Obrant, V. I. Poromov, V. V. Sarantsev, G. L. Sokolov, and G. S. Sherman, Nucl. Phys. **A414**, 479 (1984).
[16] J. Arvieux *et al.*, Nucl. Phys. **A444**, 579 (1985).
[17] M. A. Moinester *et al.*, in *Panic '87,* Proceedings of the XI International Conference on Particles and Nuclei, Kyoto, 1987, edited by S. Homma *et al.* [Nucl. Phys. **A478** (1988)], Abstract Book I, p. c72.
[18] M. A. Khandaker, M. Doss, I. Halpern, T. Murakami, D. W. Storm, D. R. Tieger, and W. A. Burger, Phys. Rev. C **44**, 24 (1991).
[19] H. Garcilazo, Phys. Rev. C **35**, 1804 (1987).
[20] F. Gross, Phys. Rev. C **26**, 2226 (1982).
[21] H. Nielsen and G. C. Oades, Nucl. Phys. **B49**, 573 (1972).
[22] H. Nielsen, J. L. Petersen, and E. Pietarinen, Nucl. Phys. **B22**, 525 (1970).
[23] R. Blankenbecler and L. F. Cook, Jr., Phys. Rev. **119**, 1745 (1960).
[24] M. Gourdin, M. Le Bellac, F. M. Renard, and J. Tran Thanh Van, Nuovo Cimento **37**, 524 (1965).
[25] W. W. Buck and Franz Gross, Phys. Rev. D **20**, 2361 (1979).
[26] J. D. Bjorken and S. D. Drell, *Relativistic Quantum Mechanics* (McGraw-Hill, New York, 1964).
[27] M. Lacombe, B. Loiseau, R. Vinh Mau, J. Côté, P. Pirés, and R. R. de Tourreil, Phys. Lett. **101B**, 139 (1981).
[28] J. Haidenbauer and W. Plessas, Phys. Rev. C **30**, 1822 (1984).
[29] M. Jacob and G. C. Wick, Ann. Phys. (N.Y.) **7**, 404 (1959).
[30] G. C. Wick, Ann. Phys. (N.Y.) **18**, 65 (1962).
[31] H. Garcilazo, J. Math. Phys. **27**, 2583 (1986).
[32] M. Simonius, in *Polarization Nuclear Physics,* edited by D. Fick, Lecture Notes in Physics Vol. 30 (Springer, Berlin, 1974), p. 38.
[33] E. T. Boschitz, private communication.
[34] R. Machleidt, K. Holinde, and Ch. Elster, Phys. Rep. **149**, 1 (1987).
[35] H. Garcilazo, Phys. Rev. Lett. **65**, 293 (1990).